ARTICLES
PUBLISHED ONLINE: 25 MARCH 2012 | DOI: 10.1038/NPHYS2276
nature physics

# The energy–speed–accuracy trade-off in sensory adaptation

Ganhui Lan[1†‡], Pablo Sartori[2‡], Silke Neumann[3], Victor Sourjik[3] and Yuhai Tu[1*]

**Adaptation is the essential process by which an organism becomes better suited to its environment. The benefits of adaptation are well documented, but the cost it incurs remains poorly understood. Here, by analysing a stochastic model of a minimum feedback network underlying many sensory adaptation systems, we show that adaptive processes are necessarily dissipative, and continuous energy consumption is required to stabilize the adapted state. Our study reveals a general relation among energy dissipation rate, adaptation speed and the maximum adaptation accuracy. This energy–speed–accuracy relation is tested in the *Escherichia coli* chemosensory system, which exhibits near-perfect chemoreceptor adaptation. We identify key requirements for the underlying biochemical network to achieve accurate adaptation with a given energy budget. Moreover, direct measurements confirm the prediction that adaptation slows down as cells gradually de-energize in a nutrient-poor medium without compromising adaptation accuracy. Our work provides a general framework to study cost-performance trade-offs for cellular regulatory functions and information processing.**

Living systems are highly dissipative, consuming energy to carry out different vital functions. Although it is natural to relate energy consumption to physical functions in a cell, such as biomolecule synthesis and cell motility, the costs of regulatory functions, from maintaining homeostasis to timing of the cell cycle to computing in the brain[1], remain poorly understood. Sensory adaptation is an important regulatory function possessed by many living systems. It allows organisms to adjust themselves to maintain their sensitivity and fitness in varying environments. Most sensory adaptations are facilitated by biochemical feedback networks, examples of which, in systems ranging from bacterial chemotaxis[2] and osmotic sensing in yeast[3] to olfactory[4] and light sensing[5] in mammalian sensory neurons, are shown in Fig. 1. Given the small number of molecules in the underlying chemical reactions and thermal fluctuations, the dynamics of biological networks are inherently noisy. This then raises the questions of what drives accurate adaptation in noisy biological systems and what is the energy cost of the biochemical feedback control mechanisms.

We address these questions by first studying the stochastic dynamics of the core negative feedback control loop (Fig. 1a) shared by various adaptation systems (Fig. 1b–e). We show that despite their varying complexities, negative feedback control mechanisms break detailed balance, and therefore always operate out of equilibrium with energy dissipation. We find that energy dissipation is needed to stabilize the adapted state against noise. A relation between adaptation performance, characterized by its speed and accuracy, and the minimum energy cost is discovered. This energy–speed–accuracy (ESA) relationship is verified in a detailed microscopic model of the *E. coli* chemosensory system. Direct measurements of the adaptation dynamics of starving *E. coli* cells show that adaptation slows down but maintains its accuracy, confirming our predictions. Finally, we discuss the general implications of our study and its comparison with other biological information processing mechanisms (such as kinetic proofreading).

## Breakdown of detailed balance in negative feedback loop

The three-node negative feedback network shown in Fig. 1a represents a minimum network to achieve accurate adaptation[6]. A stimulus signal ($s$) causes a fast response in the output activity ($a$). The change in $a$ triggers a slower change in the negative control element ($m$), which eventually cancels the effect of $s$ and brings $a$ back to a stimulus-independent level $a_0$. Owing to the small size of a cell, *in vivo* biochemical reactions are highly noisy. The stochastic dynamics of this feedback network can be described by two coupled Langevin equations[7]:

$$\dot{a} = F_a(a,m,s) + \eta_a(t); \qquad \dot{m} = F_m(a,m) + \eta_m(t) \tag{1}$$

The functions $F_a$ and $F_m$ characterize the coarse-grained biochemical interactions, $\eta_a$ and $\eta_m$ are the noises, assumed to be white with strengths $2\Delta_a$ and $2\Delta_m$ respectively. The detailed balance condition $\Delta_m \partial_m F_a = \Delta_a \partial_a F_m$ is satisfied in all equilibrium systems[8]. However, the negative feedback mechanism for adaptation requires the two cross derivatives of the interaction functions, $\partial F_a/\partial m$ and $\partial F_m/\partial a$, to have opposite signs. This requirement directly indicates the breakdown of detailed balance in all negative feedback control systems. This means that adaptation is necessarily a non-equilibrium process and it always costs (dissipates) energy.

To understand why energy dissipation is necessary for adaptation, we consider the following forms of $F_a$ and $F_m$:

$$F_a(a,m,s) = -\omega_a[a - G(s,m)] \tag{2}$$

$$F_m(a,m) = -\omega_m(a-a_0)[\beta - (1-\beta)C\partial G(s,m)/\partial m] \tag{3}$$

Here, $F_a$ describes the fast response dynamics of $a$, with a fast rate $\omega_a$; $G(s,m)$ is the mean activity with opposite dependence on $s$ and $m$ ($\partial_m G > 0$, $\partial_s G < 0$). $F_m$ describes the slow adaptation dynamics, with the adaptation speed controlled by $\omega_m (\ll \omega_a)$. The

[1]IBM T.J. Watson Research Center, PO Box 218, Yorktown Heights, New York 10598, USA, [2]Max Planck Institute for the Physics of Complex Systems, Nothnitzer Str. 38, 01187 Dresden, Germany, [3]Zentrum fur Molekulare Biologie der Universitat Heidelberg, 69120 Heidelberg, Germany. †Present address: NCI Physical Sciences—Oncology Center, Johns Hopkins University, 3400 N Charles St., Maryland 21218, USA. ‡These authors contributed equally to this work. *e-mail: yuhai@us.ibm.com.

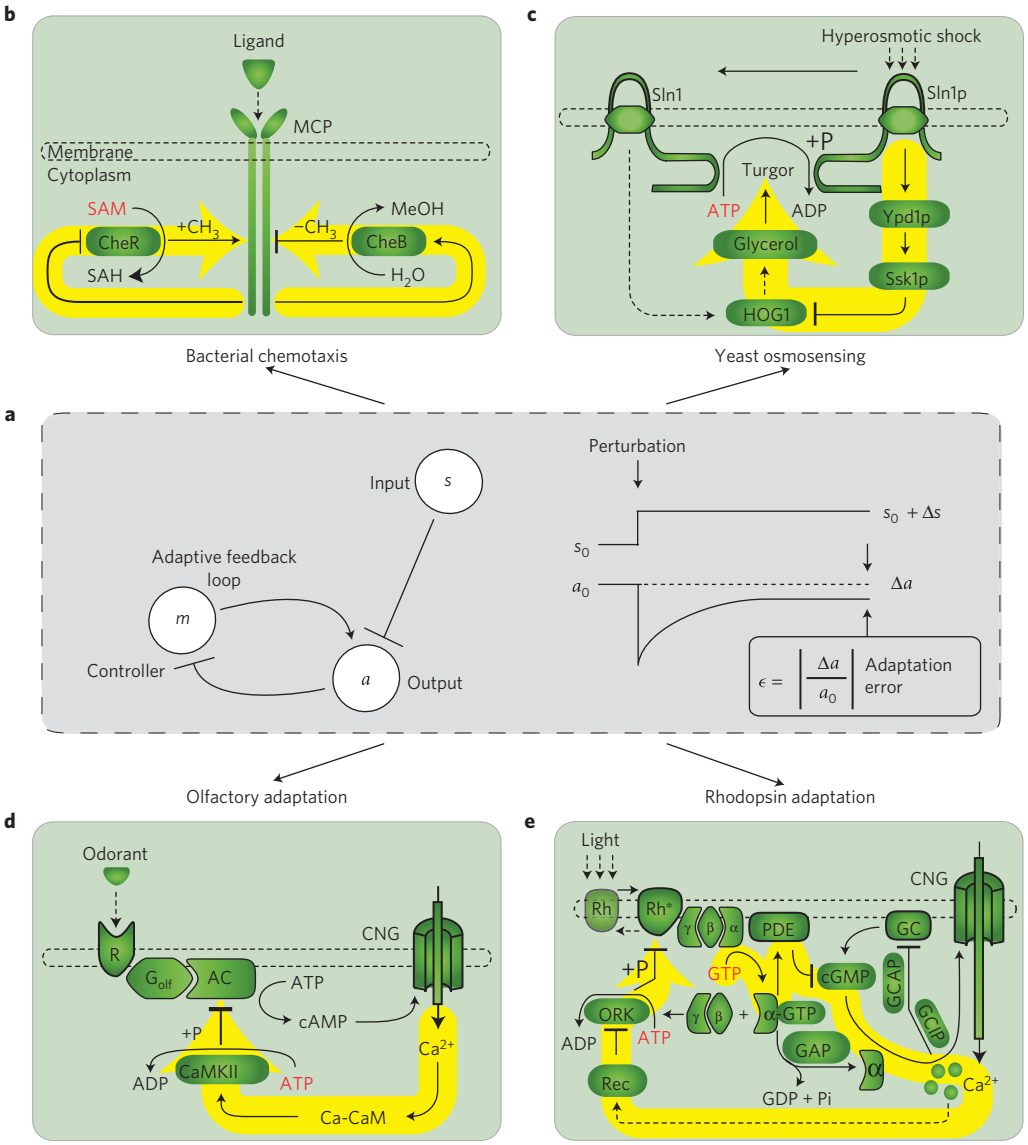


**Figure 1 | Schematic model of adaptive feedback systems. a**, The three-node feedback topology and its general adaptive behaviour. The inhibitory effect of the input is chosen arbitrarily and does not affect any of the conclusions in this paper. **b**–**e**, Examples of sensory adaptive networks with highlighted key negative feedback loops. **b**, *E. coli* chemotaxis: association of ligand to methyl-accepting chemotaxis protein (MCP) induces the methyltransferase (CheR)/methylesterase (CheB) to add/remove methyl-groups to/from MCP respectively to counteract the influence of ligand binding. **c**, Osmotic sensing in yeast: hyperosmotic shock deactivates the osmosensor Sln1p to Sln1, which stops the multi-step phospho-relay and activates the high osmolarity glycerol (HOG1) pathway to restore cell turgidity and eventually enhance the phosphorylation of Sln1 back to active Sln1p. **d**, Olfactory sensing in mammalian neurons: odorant binding induces activation of adenylyl cyclase (AC) causing the inbound calcium ($Ca^{2+}$) flux, and calmodulin (CaM) interacts with enriched calcium to form Ca-CaM and activate AC phosphorylase calmodulin kinase II (CAMKII) that eventually phosphorylates and deactivates AC. **e**, Light sensing in mammalian neurons: light activates the G-protein coupled receptor (photon-sensor) that decreases the cellular level of cyclic guanosine monophosphate (cGMP) and inhibits the inbound calcium ($Ca^{2+}$) flux, which eventually turns on the octopus rhodopsin kinase (ORK) to phosphorylate and deactivate the photon-sensor. The key high-energy biomolecules are labelled in red.

factor $(a - a_0)$ in $F_m$ is introduced to make accurate adaptation at $a = a_0$ (independent of $s$) possible. A $\beta$-dependent term (in brackets) is introduced in $F_m$ to study both the equilibrium ($\beta = 0$) and the non-equilibrium ($\beta \neq 0$) cases within the same model. For $\beta = 0$, equations (2) and (3) represent an equilibrium model, as the detailed balance condition is satisfied with the constant $C = \Delta_m\omega_a/(\Delta_a\omega_m)$. For $\beta \neq 0$, the model becomes non-equilibrium. For $\beta = 1$, we have $F_m = -\omega_m(a - a_0)$, which corresponds to a linearized coarse-grained model for studying adaptation in *E. coli* chemotaxis[9].

From equations (2) and (3), there exists a steady state with a constant activity $a = a_0$ and an $m$-value given by $G(s, m^*) = a_0$ for all values of $\beta$. With a stimulus-independent activity $a_0$, this steady state has the desired characteristic of an accurately adapted state. However, linear stability analysis shows that this steady state is only stable when

$$\beta > \beta_c \equiv C\partial_m G(s, m^*)/(C\partial_m G(s, m^*) + 1) > 0$$

which clearly shows that stable adaptation can only be achieved in a non-equilibrium system. To further demonstrate this point, an effective potential $H(m)$ in $m$-space can be obtained by averaging over the fast-variable $a$ (see Supplementary Information for details). As shown in Fig. 2a, for the equilibrium case $\beta = 0$, the desired adaptation state $(m = m^*)$ is at the maximum of $H(m)$ and

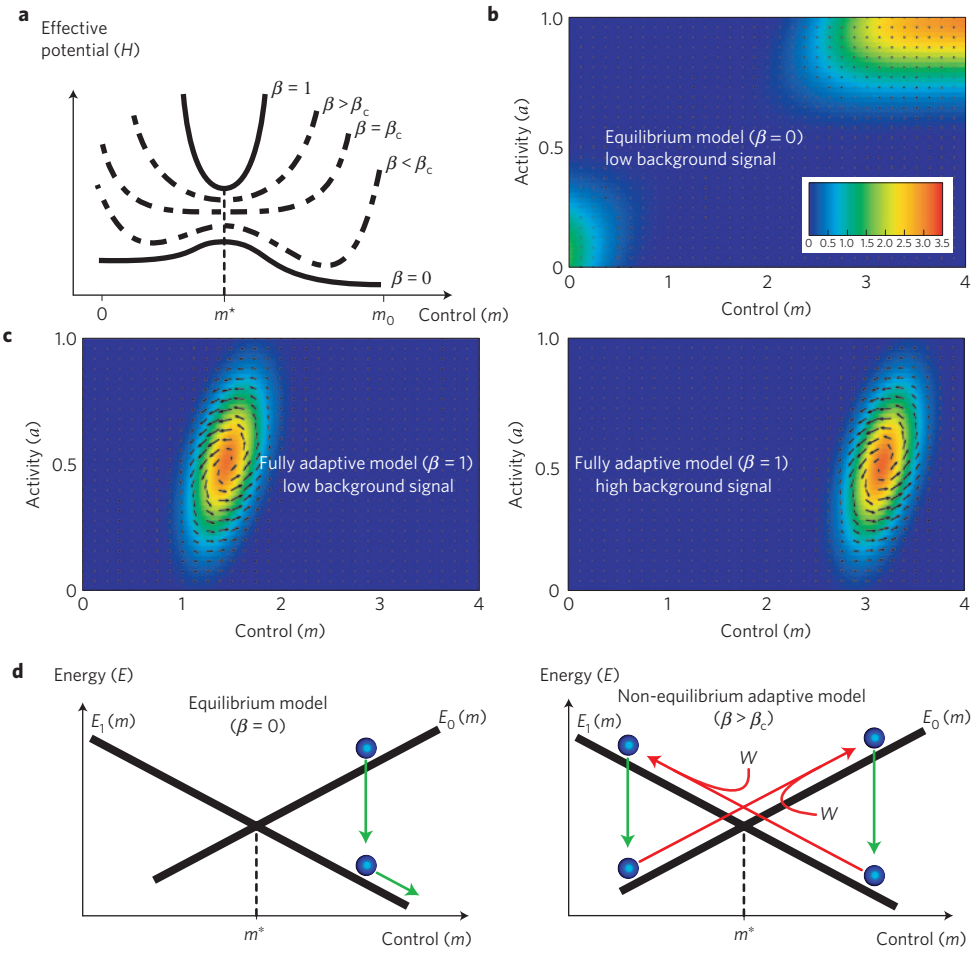


**Figure 2 | Energetics and kinetics of adaptation. a**, An effective potential, obtained by averaging over the fast activity variation, is shown for the equilibrium model ($\beta = 0$) and the non-equilibrium models ($\beta > 0$). For $\beta > \beta_c$, the state at $m = m^*$ changes from being unstable to stable. **b**, The steady-state probability density $P(a,m)$ (colour plot) and the phase-space fluxes $(J_a, J_m)$ (vector field) are shown for the equilibrium model ($\beta = 0$). The fluxes vanish $J_a = J_m = 0$ everywhere and $P(a,m)$ is centred at the corners of the phase space. **c**, In the non-equilibrium fully adaptive model ($\beta = 1$), the non-zero fluxes form a vortex (cycle) around the peak of $P(a,m)$. The peak of $P(a,m)$ has a fixed value of activity and a value of $m$ that is small for low background signal (left panel) and high for high background signal (right panel). **d**, In the equilibrium model (left panel), the system always moves downhill (green arrows) to its lowest energy state; in the non-equilibrium adaptive model (right panel), external energy ($W$) is consumed to push the system uphill (red arrows) to maintain it near the cross-over point of the active and inactive states.

therefore unstable. As $\beta$ increases, $H(m)$ is deformed, essentially by the increasing amount of energy dissipation. When $\beta > \beta_c$, $m = m^*$ becomes a minimum of $H(m)$ and stable adaptation becomes possible.

## The energy cost of adaptation

To calculate the energy cost of adaptation, we first determine the phase-space probability density $P(a,m,t)$ for the stochastic system described by equations (1)–(3). The dynamics of $P(a,m,t)$ is governed by the Fokker–Planck (FP) equation:

$$\frac{\partial P}{\partial t} = -\frac{\partial}{\partial m}\left(F_m P - \frac{\partial}{\partial m}\Delta_m P\right) - \frac{\partial}{\partial a}\left(F_a P - \frac{\partial}{\partial a}\Delta_a P\right) \equiv -\frac{\partial J_m}{\partial m} - \frac{\partial J_a}{\partial a} \quad (4)$$

where $J_a \equiv F_a P - \Delta_a(\partial P/\partial a)$ and $J_m \equiv F_m P - \Delta_m(\partial P/\partial m)$ are the two components of the probability density flux (current) in the $(a,m)$ phase-space. Following previous works[10–14], the non-equilibrium system can be characterized by its entropy production rate $\dot{S}$, which can be computed from $J_a$, $J_m$ and $P$ (see Supplementary Information for derivation). From $\dot{S}$, we obtain the rate at which the system dissipates energy by heating its environment, characterized by an effective temperature $T_{\rm eff}$:

$$\dot{W} = \int\int \left[\frac{J_a^2}{\Delta_a P} + \frac{J_m^2}{\Delta_m P}\right] {\rm d}a{\rm d}m$$

in units of $kT_{\rm eff}$, where $k$ is the Boltzmann constant. Note that the energy unit $kT_{\rm eff}$ for the coarse-grained model can be different from the thermal energy unit $kT$, even though it ultimately originates from thermal fluctuations in the underlying chemical reactions. The average activity $\langle a\rangle$ and the relative adaptation error $\epsilon$ can also be determined by $P(a,m,t)$:

$$\langle a\rangle = \int\int aP{\rm d}a{\rm d}m; \qquad \epsilon \equiv |1 - \langle a\rangle/a_0|$$

As $\omega_a \gg \omega_m$, the steady state solution $P^{(s)}(a,m)$ of the Fokker–Planck equation can be obtained approximately by separation of the fast variable $(a)$ from the slow one $(m)$. From $P^{(s)}(a,m)$, $\epsilon$ and $\dot{W}$ in the adapted state can be determined. For the biologically relevant case with $\beta = 1$ (ref. 9), we find $\epsilon \approx \epsilon_0 \exp(-c_0\omega_m/\Delta_m)$, and $\dot{W} \approx \sigma_a^2\omega_m^2/\Delta_m$, with $\sigma_a^2 \equiv \Delta_a/\omega_a$ the variance of the activity

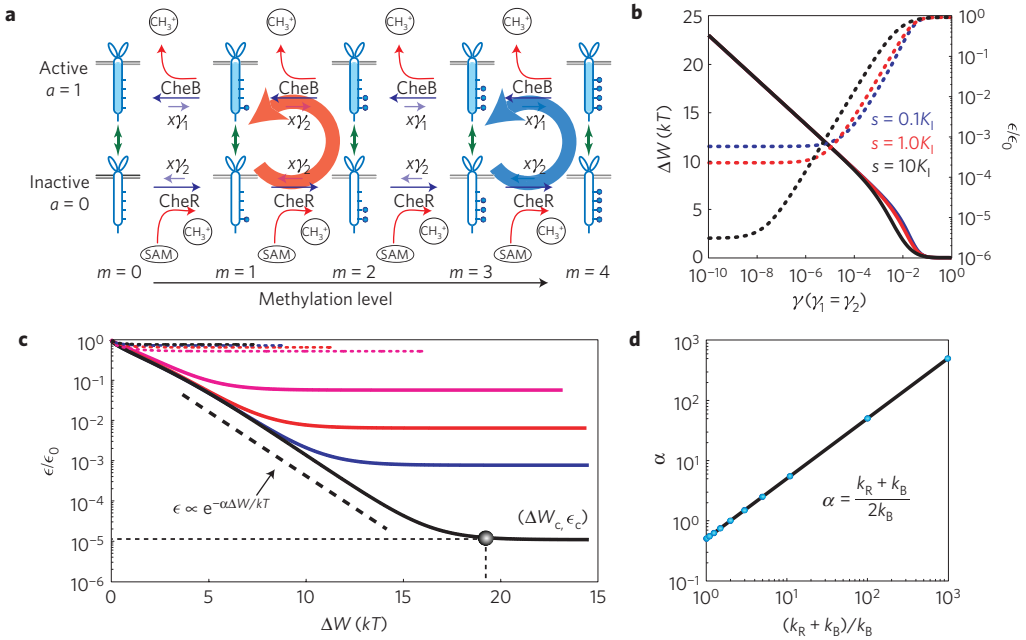


**Figure 3 | The *E. coli* chemotaxis adaptation. a**, The schematics of the *E. coli* chemoreceptor adaptation process. The red and blue cycles represent the receptor methylation–demethylation cycles for low and high attractant concentrations respectively, analogous to the flux cycles shown in Fig. 2d. **b**, The energy dissipation $\Delta W \equiv \dot{W} k_R^{-1}$ per unit of time ($k_R^{-1}$) (solid lines) and the normalized adaptation error $\epsilon/\epsilon_0$ (dotted lines) versus the parameter $\gamma$ for different values of ligand concentration $s$. $\epsilon_0 \equiv \epsilon(\gamma = 1)$. **c**, The adaptation error versus energy dissipation for different values of background ligand concentration $s$. Solid lines from bottom to top represent $\log_{10}(s/K_I) = 1.2, 1.0, 0.5, -3.0$; dashed lines from bottom to top represent $\log_{10}(s/K_I) = 3, 3.5, 4, 6$. $K_I$ is the dissociation constant for the inactive receptor. $\epsilon_c$ is the saturation error at $\Delta W \to \infty$, $\Delta W_c$ is defined as the $\Delta W$ value when $\epsilon = 0.99\epsilon_c$. **d**, The prefactor $\alpha$ in the error–energy relationship and its dependence on the methyl modification rates $k_R$ and $k_B$.

($a$) fluctuation. From these results, a simple relation between the rate of energy dissipation $\dot{W}$, the adaptation speed $\omega_m$ and the adaptation error $\epsilon$ emerges:

$$\dot{W} \approx (c_0 \sigma_a^2) \times \omega_m \times \ln(\epsilon_0/\epsilon) \tag{5}$$

where $c_0$ and $\epsilon_0$ are constants depending on the system parameters and details of $G$. This general ESA relation holds true for other cases ($\beta_c < \beta < 1$), with only different expressions for $c_0$ and $\epsilon_0$. Equation (5) clearly shows that higher energy dissipation is needed for more accurate and/or faster adaptation. See Supplementary Information for a detailed derivation of the ESA relation.

For a specific choice of $G(s, m)$ and other parameters, the phase space dynamics can be determined quantitatively by solving the FP equation (4) (see Methods). For the equilibrium model ($\beta = 0$) (Fig. 2b), the system always localizes at one of the corners of the phase space, flux vanishes everywhere ($J_a = J_m = 0$), and there is no adaptation. For the fully adaptive model ($\beta = 1$; Fig. 2c), phase-space fluxes, a trademark of non-equilibrium systems, appear. The flux vectors form a vortex (cycle) that effectively traps the system in the adapted state, which has a constant average activity ($a_0$) and an average $m$-value ($m^*$) that increases with the signal $s$ (Fig. 2c and Supplementary Movie).

The energy cost of the negative feedback control can also be understood intuitively from a two-state system that switches between its active ($a = 1$) and inactive ($a = 0$) states with free energies $E_1(m)$ and $E_0(m)$. As illustrated in Fig. 2d, $E_0(m)$ and $E_1(m)$ have different dependences on $m$ and cross at an intermediate point $m^*$ (a specific form of $E_{0,1}(m)$ is given in Methods). If the system operates at equilibrium, it always goes to its lowest energy state (Fig. 2d, left panel) and thus does not adapt. The strategy for adaptation is to trap the system near $m^*$. As the cross-point $m^*$ is not a minimum on either energy line, external free energy is consumed to push the system up the energy 'hills' along the $m$-coordinate to stabilize this adapted state (Fig. 2d, right panel).

## The energy–speed–accuracy tradeoff in *E. coli* chemotaxis

To test the general ESA relation established by the coarse-grained model of adaptation, we turn to *E. coli* chemotaxis, where detailed microscopic models are available[15–19]. Here, we use such a microscopic model to study the energy cost of adaptation and compare the results with the general ESA relation as well as with direct experimental observations.

As shown in Fig. 3a, the state of a chemoreceptor dimer is characterized by two discrete variables: $a = 0, 1$ for activity; and $m = 0, 1, \ldots, m_0$ for methylation level ($m_0 = 4$ in this paper). For a given $m$, the transitions between the active ($a = 1$) and inactive ($a = 0$) states are fast, with a characteristic timescale $\tau_a$; the mean activity is determined by the free energy difference $\Delta E(s, m)$ between active and inactive states. On a change in external signal $s$, the mean activity changes quickly. The receptors adapt by changing their methylation levels ($m$ values) to balance the effect of $s$ in $\Delta E(s, m)$. The methylation and demethylation reactions are catalyzed by the methyltransferase CheR and the methylesterase CheB respectively. Here, we approximate the methylation and demethylation processes as one-step reactions, without explicitly modelling the intermediate enzyme–substrate binding/unbinding steps. The one-step reaction rates, $k_R$ and $k_B$, depend on the enzyme and substrate concentrations. This approximation does not affect the energy dissipation rate calculation significantly for Michaelis–Menten type reactions, where the substrate reaches fast chemical equilibrium with the enzyme–substrate complex (see Supplementary Information for details). To achieve accurate adaptation, CheR should preferentially enhance the methylation of the inactive receptors and CheB should preferentially enhance the demethylation of the active receptors[15–18]. These irreversible effects are described by two parameters $\gamma_1$ ($\leq 1$) and $\gamma_2$ ($\leq 1$)

that suppress the demethylation rate for the inactive receptors and the methylation rate for the active receptors respectively from their equilibrium values.

We study the stochastic dynamics of the chemoreceptors for different values of $\gamma \leq 1$ ($\gamma_1 = \gamma_2 = \gamma$ for simplicity), where $\gamma = 1$ corresponds to the equilibrium case. The probability of a receptor in a given state $(a, m)$, $P_a(m)$, can be determined by solving the master equation. From $P_a(m)$ and the transition rates between different states, we can compute the adaptation error $\epsilon$ and the energy dissipation rate $\dot{W}$ (see Methods for details). In Fig. 3b, we show the dependence of $\epsilon$ and $\Delta W \equiv \dot{W} k_R^{-1}$, which is the energy dissipation by a receptor to its environment in the form of heat during the methylation time $\tau_R \equiv k_R^{-1}$, on $\gamma$ for different background signals. Smaller $\gamma$ leads to smaller error, but costs more energy. By plotting $\epsilon$ versus $\Delta W$ in Fig. 3c, we find that $\epsilon$ decreases exponentially with $\Delta W$ when $\Delta W$ is less than a critical value $\Delta W_c$:

$$\epsilon \approx \epsilon_0 e^{-\alpha \Delta W} \quad (6)$$

For $\Delta W > \Delta W_c$, $\epsilon$ saturates to $\epsilon_c$, which depends on key parameters of the system. The exponential error–energy relationship holds true for different choices of the kinetic rates $k_R$ and $k_B$, and the prefactor $\alpha$ is found to be: $\alpha = (k_R + k_B)/2k_B$ (Fig. 3d and Supplementary Fig. S1). With the parameter correspondence $\omega_m = k_R + k_B$, $a_0 = k_R/(k_R + k_B)$, $\sigma_a^2 = a_0(1 - a_0) = k_R k_B/(k_R + k_B)^2$ and $c_0 = 2$, equation (6) found in *E. coli* chemotaxis confirms the general ESA relationship (equation (5)).

## Network requirements for accurate adaptation

The error–energy relation (equation (6)) sets the minimum adaptation error for a given energy dissipation. To approach this optimum performance, proper conditions on the key components and parameters of the network are required. In particular, adaptation accuracy depends on the energetics and kinetics of the receptor activity, parameterized by $\Delta E(s, m)$ and activation time $\tau_a$ in our model. To evaluate these dependencies, we have computed adaptation error and energy dissipation for a large number of models, each with a random parameter set $(\Delta E(m), \tau_a, \gamma, s)$, where $\Delta E(m) \equiv \Delta E(0, m)$ is the $m$-dependent part of $\Delta E(s, m)$. The results of $\epsilon$ versus $\Delta W$ for all these models are shown in Fig. 4a. All the error–energy points are bounded by a 'best performance' (BP) line, which agrees exactly with (equation (6)).

The deviation from this BP line is caused by the finite saturation error $\epsilon_c$, evident from Fig. 3c. Taking the limit of $\gamma = 0$, we can derive the expression for $\epsilon_c$:

$$\epsilon_c = |(1/a_0 - 1)P_1(0) - P_0(m_0)|$$

which shows that the saturation error results mainly from the receptor population at the methylation boundaries ($m = 0$ or $m_0$) where the enzyme (CheB or CheR) fails to decrease or increase the receptor methylation level any further (see Supplementary Information for details). Therefore, having large boundary energy differences ($|\Delta E(0)|$, $|\Delta E(m_0)|$) and fast activation time ($\tau_a \ll k_R^{-1}$) can reduce $\epsilon_c$ by decreasing the receptor populations at the methylation boundaries (see Supplementary Figs S2,S3 for details). These requirements for accurate adaptation are met for the aspartate receptor Tar, which has $\Delta E(0) \geq 2kT$, $\Delta E(4) \leq -6kT$ (ref. 20), and $\tau_a k_R < 10^{-3}$ (ref. 2). Our analysis also provides a plausible explanation (smaller $|\Delta E(m_0)|$) for the less accurate adaptation for the serine receptor Tsr (ref. 21).

## The energy sources for adaptation

An examination of different adaptation networks (Fig. 1) shows that the energy sources are energy-bearing biomolecules such as ATP, GTP and SAM. For example, both the HOG1 feedback loop[3,22,23] in yeast osmotic shock adaptation (Fig. 1c) and the

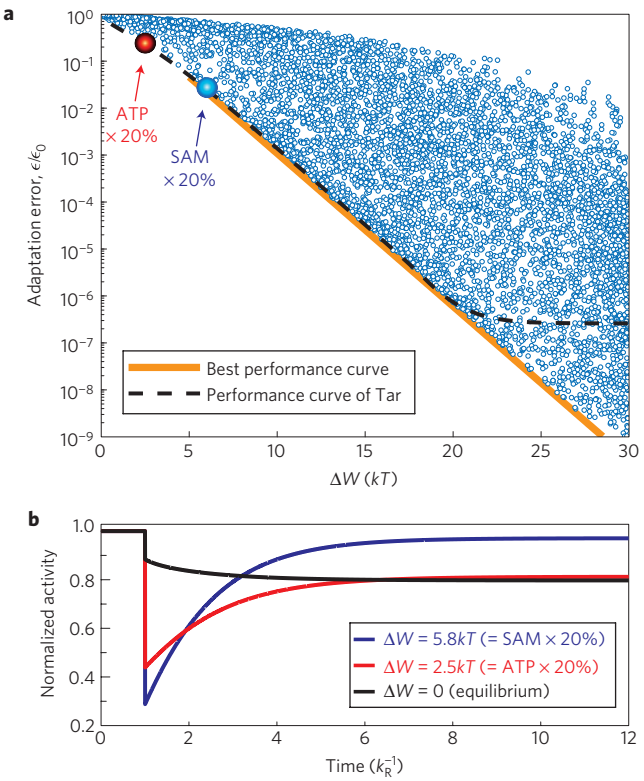


**Figure 4 | The cost–performance relationship. a**, Adaptive accuracy versus energy cost for over 10,000 different models (represented by open circles) with random choices of parameters. $\log_{10}\gamma$ is randomly picked from $[0, -10]$, $\log_{10}\tau_a$ is randomly picked from $[-3, 3]$, $\Delta E(0)$ and $-\Delta E(m_0)$ are randomly picked from $[11, 22]kT$, $\log_{10}(s/K_I)$ is randomly picked from $[-10, 10]$. The best performance line is outlined. The case for Tar is shown (dashed line) with the available energies in SAM and ATP (both at 20% efficiency) marked. **b**, The responses to a step stimulus (from $s = 0$ to $s = 10K_I$) at $t = 1$ for the equilibrium model (black), and non-equilibrium models driven by ATP (red line) and SAM (blue line) at 20% efficiency.

Calmodulin kinase II-dependent feedback control[4,24,25] for olfactory adaptation (Fig. 1d) are fueled by ATP hydrolysis accompanying various phosphorylation–dephosphorylation cycles.

For *E. coli* chemotaxis, adaptation is driven by hydrolysis of SAM, the methyl group donor for chemoreceptors. Because one fuel molecule (SAM) is hydrolyzed during each methylation–demethylation cycle, the adaptation accuracy is controlled by the free energy release in the hydrolysis of one fuel molecule. As shown in Fig. 4b, given the high energy release ($\Delta G^0 \sim 29kT$) from methylation by SAM (ref. 26), a modest 20% efficiency ($\Delta W/\Delta G^0$) leads to a maximum adaptation accuracy of ~99%, consistent with the high adaptation accuracy observed in *E. coli* chemotaxis[27]. At the same efficiency, if adaptation is driven by phosphorylation from ATP ($\Delta G^0 \sim 12kT$), the accuracy would be ~80%, consistent with the less accurate (but adequate) adaptation in the rod cell[5,28].

## Adaptation dynamics of starving cells

According to the ESA relation, the adaptation accuracy is controlled by the dissipated free energy, which comprises two parts: the internal energy of the fuel molecule and an entropic contribution. As the entropic energy depends only on the logarithm of the fuel molecule concentration, the adaptation accuracy is not very sensitive to the change in abundance of the fuel molecule. However, the kinetic rates, for example the methylation rate $k_R$, depend strongly on the concentration of the fuel molecule. Therefore, if a cell's fuel molecule pool becomes smaller owing to deficient

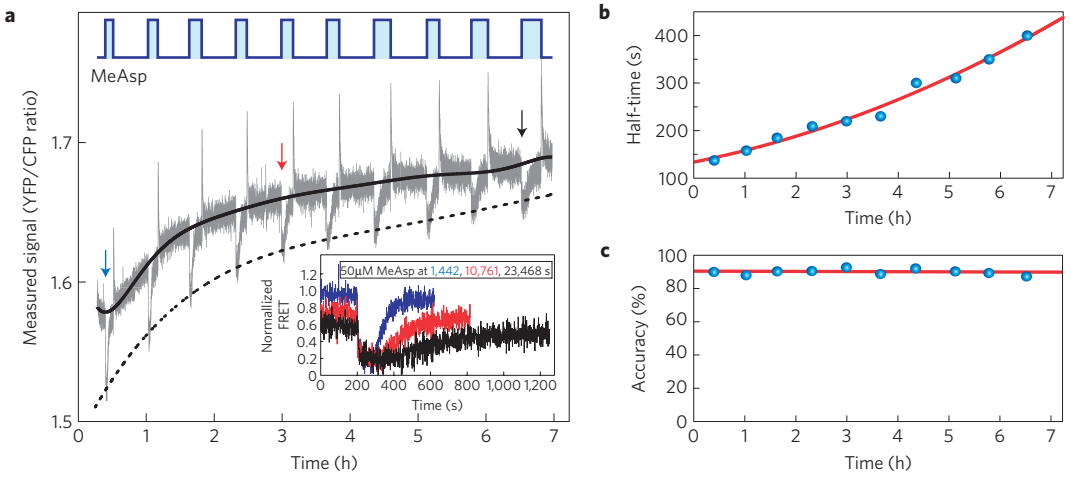


**Figure 5 | Adaptation dynamics of starving *E. coli* cells. a**, Response of *E. coli* cells to successive addition and removal of a saturating stimulus (50 μM MeAsp) over a 7 h period in a medium without nutrition (stimulus time series shown at top). Changes in kinase activity were measured using a FRET reporter based on a YFP fusion to the chemotaxis response regulator CheY and a CFP fusion to its phosphatase CheZ. The grey line is the monitored ratio of YFP to CFP fluorescence. The baseline YFP/CFP ratio at zero FRET is shown by the black dashed line. The black solid line indicates the adapted activity without any stimuli. The drift in the zero-FRET baseline is primarily due to the differences in the photobleaching kinetics of YFP and CFP. The inset plot shows the normalized FRET signal in response to 50 μM MeAsp addition at 1,442 s (blue), 10,761 s (red) and 23,468 s (black), as indicated by arrows of the same colours in the main plot. The response amplitude weakens as cells de-energize. Adaptation takes longer, but activity always returns to its pre-stimulus level with high accuracy. **b**, The adaptation half-time, defined as the time needed to recover half of the maximum response on MeAsp addition, increases by a factor of about three (from ∼130 s to ∼410 s). **c**, The relative adaptation accuracy remains unchanged (∼ 95%). The symbols in **b** and **c** are from measurements and the red lines are a guide for the eye.

metabolism or starvation, the adaptation should slow down whereas its accuracy should stay relatively unaffected.

We have tested this prediction by direct measurements of *E. coli*'s adaptation dynamics using fluorescent resonance energy transfer (FRET; ref. 29). As shown in Fig. 5a–c, adaptation to a given stimulus becomes progressively slower (Fig. 5b) for cells that are kept in a medium without an energy source. The background kinase activity (in buffer) decreases with time (Fig. 5a), indicative of the decreasing energy level of the starving cells. Remarkably, the adaptation accuracy remains almost unchanged with time (within experimental resolution), as shown in Fig. 5c, consistent with our prediction.

For an *E. coli* cell, the methylation levels of its chemoreceptors serve as the memory of the external signals it received[30]. After a change in the signal, the adaptation process 'rewrites' this memory accordingly. As pointed out by Landauer[31], only erasure of information (for example, memory) is dissipative owing to phase space contraction and the resulting entropy reduction. As changing the methylation level does not necessarily shrink the phase space, the adaptation response to a signal change does not have to cost extra energy. Instead, energy is consumed continuously to maintain the stability of the adapted state or, equivalently, the integrity of the memory against noise. For an *E. coli* cell with $\sim 10^4$ chemoreceptors[32] and a (linear) adaptation time of ∼10 s, the energy consumption rate is $\sim 3 \times 10^4 kT$/s (equivalent to $\sim 10^3$ ATP/s), which is 5–10% of the energy needed to drive a flagellar motor rotating at 100 Hz (ref. 33), even when the cell is not actively sensing or adapting. The total energy budget for regulations in an *E. coli* cell is higher, given the many regulatory functions needed for its survival. During starvation, *E. coli* cells are likely to have different priorities for different energy consuming functions. Thus, the slowing down of adaptation in starved cells seen in Fig. 5a may be seen as a way for the cells to conserve energy for other regulatory functions with higher priorities.

## Discussion

In biochemical networks, there are many 'futile cycles', in which two pathways run simultaneously in opposite directions dissipating chemical energy with no apparent function[34]. Here, we show that these cycles, shown in Figs 3a and 2d, are crucial in powering accurate adaptation. In general, cells need to process information accurately under noisy conditions. A well-known example is the kinetic proofreading (KP) scheme for error-correction proposed by Hopfield[35]. Similar to the sensory adaptation system studied here, energy is also consumed to increase accuracy in the KP scheme[36–38]. However, subtle differences exist between adaptation and KP. Whereas energy is consumed in KP to effectively lower the free energy of the already stable 'correct' state to reduce error, it is used in the adaptation system to stabilize an originally unstable state (Fig. 2a). It remains an open question whether there are general thermodynamic principles governing cellular information processing, such as proofreading and sensory adaptation. It will also be interesting to establish the ESA relationship in other more complex adaptation systems, such as those mentioned in Fig. 1c–e, and to relate the ESA relationship to the efficiency at maximum power studied in molecular motor systems[11,39].

Biological systems consume energy to carry out various vital functions, many of which are related to regulation[40], where accuracy and speed are of primary importance. Despite the complexity of biochemical networks responsible for various regulatory functions, it has been suggested that a small set of network motifs are used repeatedly[41]. The cost–performance tradeoff studied in this paper provides a new perspective, in addition to other general considerations such as robustness[15] and evolvability[42], to understand the design principles and evolutionary origins of these regulatory circuits and their building blocks.

## Methods

**A specific case of $G(s, m)$.** A simple sigmoidal form $G(s,m) = 1/[1+(s/K_d(m))^H]$ has been studied in the continuum adaptation model, equations (1)–(3), with $K_d(m) = K_0 e^{2m}$ and $K_0 = 1$ setting the scale for $s$. For the results shown in Fig. 2c–d, the Fokker Planck equation (equation (4)) is solved in the region $0 \le a \le 1$, $0 \le m \le 4$ with the grid size $da = 0.02$, $dm = 0.025$ and time step $dt = 5 \times 10^{-4}$. No flux boundary conditions are used: $J_m(a, m=0) = J_m(a, m=4) = J_a(a=0, m) = J_a(a=1, m) = 0$. Other parameters used are $\omega_m = 5$, $\omega_a = 50 (\gg \omega_m)$, $\sigma_a^2 = \sigma_m^2 = 10^{-2}$, $a_0 = 0.5$, and $H = 1$.

**Details of the *E. coli* chemoreceptor adaptation model.** The free energy difference $\Delta E(s,m) = E_1(m) - E_0(m) = Ne_m(m_1 - m) + N(\ln[[1+s/K_1]/[1+s/K_A]])$ is taken from the Monod–Chandeux–Wyman (MWC) model of *E. coli* chemoreceptor complexes[9], with $s$ the ligand concentration. We choose $E_a(s,m) = (a-1/2)\Delta E(s,m)$ for simplicity. The parameters in $\Delta E(s,m)$ are from ref. 9 for *E. coli* chemoreceptor Tar : $K_1 = 18.2\,\mu$M, $K_A = 3{,}000\,\mu$M, $e_m = 2$, $m_1 = 1$. $N$ is the number of strongly coupled receptor dimers. From the linear dependence of $\Delta E$ on $N$, it can be shown that the energy dissipation rate $\dot{W}$ scales linearly with $N$. So only $N = 1$ is studied here and the resulting energy cost is for each receptor dimer. Note that according to ref. 20, the adaptation speed also scales linearly with $N$. Therefore, the ESA relation holds independent of $N$.

The dynamics of $P_a(m)$ is governed by the master equation: $\mathrm{d}P_a(m)/\mathrm{d}t = k_{-,a}(m+1)P_a(m+1) + k_{+,a}(m-1)P_a(m-1) + \omega_{1-a}(m)P_{1-a}(m) - (k_{-,a}(m) + k_{+,a}(m) + \omega_a(m))P_a(m)$, for $a = 0, 1$ and $m = 0, 1, 2, 3, 4$. No (transition) flux boundary conditions are used at $m = 0$ and $m = 4$. The methylation (demethylation) rate for inactive (active) receptor is set to be $k_R$ and $k_B$: $k_{+,0}(m) = k_R$, $k_{-,1}(m) = k_B$. Their counter rates are suppressed from their equilibrium values by $\gamma_1$ and $\gamma_2$: $k_{-,0}(m) = k^{eq}_{-,0}(m) \times \gamma_1 = k_R \exp[-Ne_m/2]\gamma_1$, $k_{+,1}(m) = k^{eq}_{+,1}(m) \times \gamma_2 = k_B \exp[-Ne_m/2]\gamma_2$. The activation rate $\omega_0(m)$ and deactivation rate $\omega_1(m)$ satisfy $\omega_1(m) = \omega_0(m)\exp[\Delta E(s,m)]$. The activation time $\tau_a \equiv [\min(\omega_1(m), \omega_0(m))]^{-1}$ is set to be $10^{-3}$, much faster than the methylation time $\tau_R \equiv 1/k_R$ set by $k_R = 1$.

The steady-state distribution $P^{(s)}_a(m)$ is solved by $\mathrm{d}P^{(s)}_a(m)/\mathrm{d}t = 0$. The energy dissipation depends on the fluxes between two states $A$ and $B$. For example, for $A = (a,m)$, $B = (a,m+1)$, the two counter fluxes are $J_{AB} = k_{+,a}(m)P^{(s)}_a(m)$ and $J_{BA} = k_{-,a}(m+1)P^{(s)}_a(m+1)$. The entropy production rate at link $AB$ is $\dot{S}_{AB} = (J_{AB} - J_{BA})\ln[J_{AB}/J_{BA}]$, and the total entropy production rate $\dot{S}$ of the system is the sum of $\dot{S}_{AB}$ over all the links (see Supplementary Information for details). The energy dissipation rate $\dot{W} = kT\dot{S}$, where $kT$ is the thermal energy unit. The adaptation error can be obtained from the average activity $\langle a \rangle = \sum_m P^{(s)}_1(m)$.

**Experiments.** The adaptation measurement was performed with tryptone broth-grown *E. coli* K-12 strain LJ110 Δ (*cheY cheZ*) expressing the CheY-YFP (yellow fluorescent protein)/CheZ-CFP (cyan flourescent protein) FRET pair, a reporter for kinase activity, as described in a previous article[43]. During the measurement, cells were kept under a constant flow of nutrient-free tethering buffer (10 mM $KPO_4$, 0.1 mM EDTA, 1 μM methionine, 67 mM NaCl, pH7) at a rate of 300 μl min$^{-1}$ and were stimulated at regular intervals with 50 μM α-methyl-DL-aspartate (MeAsp), a non-metabolizable aspartate analogue, until adaptation was completed. Data were acquired as in ref. 43.

Received 9 September 2011; accepted 22 February 2012; published online 25 March 2012

## References


1. Niven, J. E. & Laughlin, S. B. Energy limitation as a selective pressure on the evolution of sensory systems. *J. Exp. Biol.* **211,** 1792–1804 (2008).
2. Hazelbauer, G. L., Falke, J. J. & Parkinson, J. S. Bacterial chemoreceptors: high-performance signaling in networked arrays. *Trends Biochem. Sci.* **33,** 9–19 (2008).
3. Hohmann, S. Osmotic stress signaling and osmoadaptation in yeasts. *Am. Soc. Microbiol.* **66,** 300–372 (2002).
4. Menini, A. Calcium signalling and regulation in olfactory neurons. *Curr. Opinion Neurobiol.* **9,** 419–426 (1999).
5. Nakatani, K., Tamura, T. & Yau, K. W. Light adaptation in retinal rods of the rabbit and two other nonprimate mammals. *J. Gen. Physiol.* **97,** 413–435 (1991).
6. Ma, W. *et al.* Defining network topologies that can achieve biochemical adaptation. *Cell* **138,** 760–773 (2009).
7. Sartori, P. & Tu, Y. Noise filtering strategies in adaptive biochemical signaling networks: Application to *E. Coli* chemotaxis. *J. Stat. Phys.* **142,** 1206–1217 (2011).
8. Kampen Van, N. G. *Stochastic Processes in Physics and Chemistry* (North-Holland, 1981).
9. Tu, Y., Shimizu, T. S. & Berg, H. C. Modeling the chemotactic response of *E. Coli* to time-varying stimuli. *Proc. Natl Acad. Sci. USA* **105,** 14855–14860 (2008).
10. Lebowitz, J. L. & Spohn, H. A Gallavotti–Cohen-type symmetry in the large deviation funcional for stochastic dynmaics. *J. Stat. Phys.* **95,** 333–365 (1999).
11. Parmeggiani, A., Julicher, F., Ajdari, A. & Prost, J. Energy transduction of isothermal ratchets: Generic aspects and specific examples close to and far from equilibrium. *Phys. Rev. E* **60,** 2127–2140 (1999).
12. Seifert, U. Entropy production along a stochastic trajectory and an integral fluctuation theorem. *Phys. Rev. Lett.* **95,** 040602 (2005).
13. Tome, T. Entropy production in nonequilibrium systems described by a Fokker–Planck equation. *Brazilian J. Phys.* **36,** 1285–1289 (2006).
14. Qian, H. Phosphorylation energy hypothesis: Open chemical systems and their biological functions. *Annu. Rev. Phys. Chem.* **58,** 113–142 (2007).
15. Barkai, N. & Leibler, S. Robustness in simple biochemical networks. *Nature* **387,** 913–917 (1997).
16. Morton-Firth, C. J. & Bray, D. Predicting temporal fluctuations in an intracellular signalling pathway. *J. Theor. Biol.* **192,** 117–128 (1998).
17. Yi, T. M. *et al.* Robust perfect adaptation in bacterial chemotaxis through integral feedback control. *Proc. Natl Acad. Sci. USA* **97,** 4649–4653 (2000).
18. Mello, B. A. & Tu, Y. Perfect and near perfect adaptation in a model of bacterial chemotaxis. *Biophys. J.* **84,** 2943–2956 (2003).
19. Endres, R. G. & Wingreen, N. S. Precise adaptation in bacterial chemotaxis through assistance neighborhoods. *Proc. Natl Acad. Sci. USA* **103,** 13040–13044 (2006).
20. Shimizu, T. S., Tu, Y. & Berg, H. C. A modular gradient-sensing network for chemotaxis in *Escherichia Coli* revealed by responses to time-varying stimuli. *Mol. Syst. Biol.* **6,** 382 (2010).
21. Berg, H. C. & Brown, D. A. Chemotaxis in *Escherichia coli* analysed by three-dimensional tracking. *Nature* **239,** 500–504 (1972).
22. Ota, I. M. & Varshavsky, A. A yeast protein similar to bacterial two-component regulators. *Science* **262,** 566–569 (1993).
23. Posas, F. *et al.* Yeast HOG1 MAP kinase cascade is regulated by a multistep phosphorelay mechanism in the SLN1-YPD1-SSK1 two-component' osmosensor. *Cell* **86,** 865–875 (1996).
24. Zufall, F., Shepherd, G. M. & Firestein, S. Inhibition of the olfactory cyclic nucleotide gated ion channel by intracellular calcium. *Proc. Biol. Sci.* **246,** 225–230 (1991).
25. Matthews, H. R. & Reisert, J. Calcium, the two-faced messenger of olfactory transduction and adaptation. *Curr. Opin. Neurobiol.* **13,** 469–475 (2003).
26. Walsh, C. *Posttranslational Modification of Proteins: Expanding Nature's Inventory* (Roberts & Company Publishers, 2006).
27. Alon, U. *et al.* Robustness in bacterial chemotaxis. *Nature* **397,** 168–171 (1999).
28. Detwiler, P. B. *et al.* Engineering aspects of enzymatic signal transdcusion: Photoreceptors in the retina. *Biophys. J.* **79,** 2801–2817 (2000).
29. Sourjik, V. & Berg, H. C. Receptor sensitivity in bacterial chemotaxis. *Proc. Natl Acad. Sci. USA* **99,** 123–127 (2002).
30. Lan, G. *et al.* Adapt locally and act globally: Strategy to maintain high chemoreceptor sensitivity in complex environments. *Mol. Syst. Biol.* **7,** 475 (2011).
31. Landauer, R. Dissipation and noise immunity in computation and communication. *Nature* **335,** 779–784 (1988).
32. Li, M. & Hazelbauer, G. L. Cellular stoichiometry of the components of the chemotaxis signaling complex. *J. Bacteriol.* **186,** 3687–3694 (2004).
33. Berg, H. C. The rotary motor of bacterial flagella. *Ann. Rev. Biochem.* **72,** 19–54 (2003).
34. Voet, D., Voet, J. G. & Pratt, C. W. *Fundamentals of Biochemistry* (Wiley, 1999).
35. Hopfield, J. J. Kinetics proofreading: a new mechanism for reducing errors in biosynthetic processes requiring high specificity. *Proc. Natl Acad. Sci. USA* **71,** 4135–4139 (1974).
36. Savageau, M. A. & Freter, R. R. Energy cost of proofreading to increase fidelity of transfer ribonucleic acid aminoacylation. *Biochemistry* **18,** 3486–3493 (1979).
37. Bennett, C. H. Dissipation-error tradeoff in proofreading. *Biosystems* **11,** 85–91 (1979).
38. Qian, H. Reducing intrinsic biochemical noise in cells and its thermodynamic limit. *J. Mol. Biol.* **362,** 387–392 (2006).
39. Schmidel, T. & Seifert, U. Efficiency of molecular motors at maximum power. *Europhys. Lett.* **83,** 30005 (2008).
40. Koshland, D. E., Goldbeter, A. & Stock, J. B. Amplification and adaptation in regulatory and sensory systems. *Science* **217,** 220–225 (1982).
41. Alon, U. *An Introduction to Systems Biology: Design Principles of Biological Circuits* (CRC Press, 2007).
42. Kashtan, N. & Alon, U. Spontaneous evolution of modularity and network motifs. *Proc. Natl Acad. Sci. USA* **102,** 13883–13778 (2005).
43. Neumann, S. *et al.* Differences in signalling by directly and indirectly binding ligands in bacterial chemotaxis. *EMBO J.* **29,** 3484–3495 (2010).


## Acknowledgements

We thank J. Tersoff, T. Theis and K. Schwarz for comments. This work is partially supported by a National Institutes of Health (NIH) grant (R01GM081747 to Y.T.), a Deutsche Forschungsgemeinschaft (DFG) grant (SO 421/3-3 to V.S.), and a Cajamadrid fellowship to P.S.

## Author contributions

Y.T. initiated the work; G.L., P.S. and Y.T. carried out the theoretical calculations; S.N. and V.S. performed the experiments; G.L. did the data analysis; all authors wrote the paper.

## Additional information

The authors declare no competing financial interests. Supplementary information accompanies this paper on www.nature.com/naturephysics. Reprints and permissions information is available online at www.nature.com/reprints. Correspondence and requests for materials should be addressed to Y.T.

nature physics
SUPPLEMENTARY INFORMATION
DOI: 10.1038/NPHYS2276

# The energy–speed–accuracy trade-off in sensory adaptation

## 1 The effective potential $H(m)$

In the main text, we introduced a set of $F_a$ and $F_m$ functions to study the role of energy dissipation in adaptation.

$$F_a(a,m,s) = -\omega_a[a - G(s,m)], \tag{S1}$$

$$F_m(a,m) = -\omega_m(a-a_0)[\beta - (1-\beta)\frac{\Delta_m/\omega_m}{\Delta_a/\omega_a}\partial_m G(s,m)], \tag{S2}$$

with $0 \leq a \leq 1$ and $0 \leq m \leq m_0$. $F_a$ describes the fast ($\omega_a \gg \omega_m$) relaxation dynamics of the activity $a$ to its steady state value $G(s,m)$. $G$ has opposite dependence on $s$ and $m$, e.g., $\partial_s G < 0$ and $\partial_m G > 0$ used in this study.

Before deriving the effective potential $H(m)$, we briefly explain the form of $F_m$ used here. $\beta$ is a continuous parameter ranging from 0 to 1 which changes the form of $F_m$ in order to study both equilibrium and nonequilibrium cases within the same model. To find an equilibrium interaction $F_m^{eq}$ that allows adaptation to $a_0$ we integrate the detailed balance condition ($\Delta_a^{-1}\partial_m F_a = \Delta_m^{-1}\partial_a F_m$) and use the linear form to impose $a_0$ to be a steady state ($F_m^{eq}(a_0) = 0$). This gives $F_m^{eq} = \omega_a \frac{\Delta_m}{\Delta_a}(a-a_0)\partial_m G$. For non-equilibrium reactions, which break detailed balance but still keep $a_0$ as a steady state, we use the simple linear form $F_m^{neq} = -\omega_m(a-a_0)$. Combining the equilibrium and nonequilibrium terms linearly, we have $F_m = \beta F_m^{eq} + (1-\beta)F_m^{neq}$, which is what we have used in this study.

Now we derive $H(m)$. First, we can obtain a set of approximate analytical solutions of the probability distribution $P(a,m)$ in the limit where adaptation is much slower than response $\omega_a \gg \omega_m$, where we can separate the probability distribution as $P(a,m) = P_a(a/m)P_m(m)$. By using this adiabatic approximation, we obtain

$$P_a(a/m) = \exp\left(-\frac{\omega_a}{2\Delta_a}[a - G(s,m)]^2\right), \tag{S3}$$

where the normalization constant has been absorbed in $P_m$. The distribution $P_m$ can also

be calculated in this limit by using the flux conservation in the $m$ direction:

$$\begin{aligned}\int_0^1 J_m da &= \int_0^1 \Big( -\omega_m[a-a_0][\beta-(1-\beta)\frac{\Delta_m/\omega_m}{\Delta_a/\omega_a}G']P_aP_m - \Delta_m P_a\partial_m P_m \\ &- \Delta_m P_a P_m \partial_m \log(P_a)\Big)da = \int_0^1 e^{-F}\Big( -\omega_m[a-a_0][\beta-(1-\beta)\frac{\Delta_m/\omega_m}{\Delta_a/\omega_a}G']P_m \\ &- \Delta_m\partial_m P_m + \Delta_m P_m\frac{\omega_a}{\Delta_a}[a-G]G'\Big)da \\ &\approx \sqrt{\frac{2\pi\Delta_a}{\omega_a}}\Big( -\omega_m[G-a_0][\beta-(1-\beta)\frac{\Delta_m/\omega_m}{\Delta_a/\omega_a}G']P_m - \Delta_m\partial_m P_m + 0\Big) \approx 0,\end{aligned} \tag{S4}$$

from which we have

$$P_m(m) = \frac{1}{Z}\exp\left(-H(s,m)\right), \tag{S5}$$

where

$$H(s,m) = \frac{\omega_m}{\Delta_m}\int (G(s,m)-a_0)[\beta-(1-\beta)\frac{\Delta_m/\omega_m}{\Delta_a/\omega_a}G']dm \tag{S6}$$

is the effective potential illustrated in Fig. 2a in the main text, where it is abbreviated as $H(m)$ . $Z$ is the normalization constant to be determined by $\int_0^1\int_0^{m_0} P_a(a/m)P_m(m)dadm = 1$, which gives $Z = \sqrt{2\pi\Delta_a/\omega_a}\int_0^{m_0} e^{-H(s,m)}dm$.

As shown in the main text, the effective potential $H(m)$ can have different minima depending on the value of $\beta$. There is always a fixed point at $m^*$ with fixed activity $G(s,m^*) = a_0$. However, it is unstable for small $\beta$, e.g., for $\beta = 0$. It only becomes stable when $\partial^2 H/\partial m^2|_{m^*} > 0$, i.e., when $\beta > \beta_c$. The critical value $\beta_c$ is given by $\partial^2 H/\partial m^2|_{m^*} = 0$, which leads to

$$\beta_c = \frac{\Delta_m\partial_m G(s,m^*)/\omega_m}{\Delta_m\partial_m G(s,m^*)/\omega_m + \Delta_a/\omega_a},$$

as shown in the main text. It is easy to see $\beta_c$ is between 0 and 1.

# 2 The energy dissipation rate $\dot{W}$

For a microscopic system with discrete chemical states, the free energy dissipation rate $\dot{W}$ (with thermal energy unit $kT = 1$) can be written as:

$$\dot{W} = \sum_{AB}(J_{AB} - J_{BA})\ln[J_{AB}/J_{BA}], \tag{S7}$$

where $A$, $B$ represent the discrete states and $J_{AB}$, $J_{BA}$ are the transitional rates from $A \to B$ and $B \to A$ respectively, see [1] for a recent review and derivations. The interpretation

of the above equation is clear: $J_{AB} - J_{BA}$ is the net current from state A to state B; and $\ln[J_{AB}/J_{BA}]$ is the net energy dissipation for a transition from state A to state B. In equilibrium systems, detailed balance leads to $J_{AB} = J_{BA}$ and therefore $\dot{W} = 0$. For nonequilibrium systems, detailed balance is broken $J_{AB} \neq J_{BA}$, and it is easy to show that the energy dissipation rate is positive definite $\dot{W} > 0$.

For the (coarse-grained) continuum model, $A$ and $B$ represent infinitesimal states, each of size $da \times dm$, in the phase space. For example, along the $a$-direction in the phase space, $A$ and $B$ represent two infinitesimal states that are centered at $A = (a, m)$, $B = (a + da, m)$. By discretizing the Fokker-Planck equation, we can obtain the infinitesimal fluxes between them:

$$J_{AB} = [F_a P(a, m)/da + \Delta_a P(a, m)/da^2]dadm$$

,

$$J_{BA} = [\Delta_a P(a + da, m)/da^2]dadm.$$

By plugging the two expressions above in Eq. (S7) and taking the continuum limit $da \to 0$ and $dm \to 0$, we obtain the energy dissipation rate for the continuum model used in the main text:

$$\dot{W} = \int_0^1 da \int_0^{m_0} dm[\frac{J_a^2}{\Delta_a P} + \frac{J_m^2}{\Delta_m P}]. \quad \text{(S8)}$$

This expression of energy dissipation rate (Eq. (S8)) can be derived more rigorously from phase space entropy production rate, as done in [2, 3]. The procedure is to start with the entropy $S = k \int P \log(P)$ with k the Boltzmann constant, calculate its time derivative $\dot{S}$, identify the positive term which represents the entropy production rate $\dot{S}_{prod} = k \int J_i^2/(P\Delta_i)$, and finally realize that on a steady state this entropy is dissipated to the environment as heat or dissipated energy $\dot{W} = T_{eff}\dot{S}_{prod} = kT_{eff} \int J_i^2/(P\Delta_i)$ where $T_{eff}$ is the effective temperature of the environment. From Eq. (S8), it is clear that the $\dot{W}$ is positive definite and vanishes only in equilibrium system where $J_a = J_m = 0$, i.e., the detailed balance condition, is satisfied.

# 3 The ESA relation

To calculate the adaptation error, we can integrate the steady state FP equation in $a$ and $m$ and use the resulting equation $\int_0^1 da \int_0^{m_0} dm \;\; J_m = 0$. By using the definition of $J_m = F_m P - \Delta_m \partial_m P$ and Eq. (S2) for $F_m$, the relative adaptive error $\epsilon = |\langle a \rangle - a_0|/a_0$ can be obtained:

$$\begin{aligned} \epsilon &= |\frac{1}{a_0 \beta \omega_m} \int_0^1 \Delta_m P(a, 0)da - \frac{1}{a_0 \beta \omega_m} \int_0^1 \Delta_m P(a, 4)da, \\ &+ \frac{1-\beta}{a_0 \beta} \int_0^1 da \int_0^{m_0} dm \frac{\Delta_m/\omega_m}{\Delta_a/\omega_a}(a - a_0)G'(s, m)P(a, m)| \equiv |\epsilon_1 - \epsilon_2 + \epsilon_3|, \end{aligned} \quad \text{(S9)}$$

where compact derivative notation $G'(s,m) = \partial_m G(s,m)$ will be used from now on. In the above expression for $\epsilon$, the first two integrals (defined as $\epsilon_1$ and $\epsilon_2$) constitute the boundary induced errors, and the third one (defined as $\epsilon_3$) is the bulk error. We see that the bulk error $\epsilon_3$ vanishes in the fully adaptive model where $\beta = 1$. In the following two subsections, we consider the two cases, $\beta = 1$ and $1 > \beta > \beta_c$, to derive the Energy-Speed-Accuracy (ESA) relation presented in the main text.

## 3.1 The ESA relation for $\beta = 1$

In this subsection, we study the ESA relation for the biologically relevant case of $\beta = 1$, where the "bulk" error term vanishes ($\epsilon_3 = 0$) in Eq. (S9) and we have:

$$\epsilon \;=\; |\epsilon_1 - \epsilon_2| = \frac{\Delta_m}{\omega_m a_0} \Big| \int_0^1 [P_m(m_0) - P_m(0)] e^{-F} da \Big| \approx \frac{\Delta_m \sqrt{2\pi \Delta_a/\omega_a}}{\omega_m a_0} |P_m(m_0) - P_m(0)|.$$

By using the solution from the previous section for the case $\beta = 1$, we have:

$$\epsilon_1 \;=\; \frac{\Delta_m}{\omega_m a_0} \left( \int_0^{m_0} \exp[H(s,m_0) - H(s,m)] dm \right)^{-1}, \tag{S10}$$

$$\epsilon_2 \;=\; \frac{\Delta_m}{\omega_m a_0} \left( \int_0^{m_0} \exp[H(s,0) - H(s,m)] dm \right)^{-1}. \tag{S11}$$

We now apply the steepest descend method around the adaptive minimum at $m = m^*$:

$$\int_0^{m_0} e^{-H(s,m)} dm \approx e^{-H(s,m^*)} \times \sqrt{\frac{2\pi \Delta_m}{\omega_m G'}},$$

which leads to:

$$\epsilon_1 \;=\; \frac{1}{a_0} \sqrt{\frac{\Delta_m G'}{2\pi \omega_m}} \exp[H(s,m^*) - H(s,m_0)], \tag{S12}$$

$$\epsilon_2 \;=\; \frac{1}{a_0} \sqrt{\frac{\Delta_m G'}{2\pi \omega_m}} \exp[H(s,m^*) - H(s,0)]. \tag{S13}$$

So we have

$$\epsilon = |\epsilon_1 - \epsilon_2| \approx \frac{1}{a_0} \sqrt{\frac{\Delta_m G'}{2\pi \omega_m}} e^{H(s,m^*)} |\exp[-H(s,m_0)] - \exp[-H(s,0)]|. \tag{S14}$$

For a generic value of $s$, $m^*$ is closer to one of the two boundary values $m = 0$ or $m = m_0$. Without loss of generality, we assume $m^*$ is closer to $m_0$, which means that $\epsilon_1 \gg \epsilon_2$, though both $\epsilon_1$ and $\epsilon_2$ have the same form (see later). Therefore, we have

$$\epsilon \approx \frac{1}{a_0} \sqrt{\frac{\Delta_m G'}{2\pi \omega_m}} \exp[H(s,m^*) - H(s,m_0)] = \frac{1}{a_0} \sqrt{\frac{\Delta_m G'}{2\pi \omega_m}} \exp[-\frac{\omega_m}{\Delta_m} \int_{m^*}^{m_0} G(s,m) dm]. \tag{S15}$$

Defining $\epsilon_0 \equiv \sqrt{\Delta_m G'/2\pi\omega_m a_0^2}$ and a decay constant $d \equiv \int_{m^*}^{m_0} G(s,m)dm$, the final form of the error is

$$\epsilon \approx \epsilon_0 \exp - \left[\frac{d}{\Delta_m/\omega_m}\right]. \tag{S16}$$

For $m^*$ closer to $m = 0$, $\epsilon_2$ dominates and the only change for $\epsilon$ is that $d$ would be $d = \int_0^{m^*} G(s,m)dm$.

For the fully adaptive model the energy dissipation takes the form

$$\dot{W} \approx \omega_m \frac{\Delta_a/\omega_a}{\Delta_m/\omega_m}(1 + \frac{\Delta_m/\omega_m}{\Delta_a/\omega_a}G')^2.$$

We see from this expression that reducing $\Delta_m/\omega_m$, which reduces $\epsilon$, will at the same time increase the energy dissipation rate. For small adaptation error, the leading order in $\dot{W}$ can be approximated as

$$\dot{W} \approx \omega_m \frac{\Delta_a/\omega_a}{\Delta_m/\omega_m} \tag{S17}$$

By using Eq. S16, we can relate this to the adaptation error, thus arriving at the energy-speed-accuracy (ESA) relation shown in the main text (Eq. 8):

$$\dot{W} \approx (c_0\sigma_a^2) \times \omega_m \times \ln(\frac{\epsilon_0}{\epsilon}), \tag{S18}$$

with the explicit expressions for the constants: $c_0 = d^{-1} = (\int_0^{m^*} G(s,m)dm)^{-1}$, $\sigma_a^2 = \Delta_a/\omega_a$, and $\epsilon_0 = \sqrt{\Delta_m G'/2\pi\omega_m a_0^2}$.

## 3.2 The ESA relation for $\beta_c < \beta < 1$

We now study the bulk error $\epsilon_3$ in the adaptive regime $1 > \beta > \beta_c$ by expanding the kernel of the integral for $\epsilon_3$ in Eq. (S9) to the second order before applying the steepest descend method:

$$\begin{aligned}
\epsilon_3 &\approx \frac{1-\beta}{a_0\beta}\frac{\Delta_m/\omega_m}{\Delta_a/\omega_a}\sqrt{\frac{2\pi\Delta_a}{\omega_a}}\int_0^{m_0} dm\Big([(G(s,m)-a_0)G'(s,m)]_{m=m^*}P_m(m) \\
&+ [(G(s,m)-a_0)G'(s,m)]'_{m=m^*}(m-m^*)P_m(m) \\
&+ \frac{1}{2}[(G(s,m)-a_0)G'(s,m)]''_{m=m^*}(m-m^*)^2P_m(m)\Big) \\
&\approx \frac{1-\beta}{\beta}\frac{(\Delta_m/\omega_m)^2}{\Delta_a/\omega_a}\frac{3G''}{2a_0}(\beta-(1-\beta)\frac{\Delta_m/\omega_m}{\Delta_a/\omega_a}G')^{-1},
\end{aligned} \tag{S19}$$

Where the derivatives $G'$ and $G''$ are evaluated at the (adaptive) minima $m^*$. It is easy to see from above that the bulk error $\epsilon_3$ becomes smaller as $\beta \to 1$, i.e, as the system becomes

fully adaptive. By defining a constant $e_0 = 3\frac{(\Delta_m/\omega_m)^2}{\Delta_a/\omega_a}G''/2a_0$, we have $\beta \approx 1/(1+\epsilon_3/e_0)$ when $\beta$ is close to 1.

To calculate the energy dissipation we first compute the probability currents, which can be obtained using the probability density function $P(a,m)$ obtained above. As the energy dissipation is much smaller in the $a-$direction, we only calculate the current in the $m$ direction:

$$\begin{aligned} J_m(a,m) &\approx -\omega_m[a-a_0][\beta-(1-\beta)\frac{\Delta_m/\omega_m}{\Delta_a/\omega_a}G']P - \Delta_m P\partial_m \log(P) \\ &= P(-\omega_m[a-a_0][\beta-(1-\beta)\frac{\Delta_m/\omega_m}{\Delta_a/\omega_a}G'] + \Delta_m\partial_m[F+H]) \\ &= -P\omega_m[a-a_0][\beta-(1-\beta)\frac{\Delta_m/\omega_m}{\Delta_a/\omega_a}G'] \\ &+ P\Delta_m(G'(G-a)\frac{\omega_a}{\Delta_a} + (G-a_0)[\beta-(1-\beta)\frac{\Delta_m/\omega_m}{\Delta_a/\omega_a}G']\frac{\omega_m}{\Delta_m}). \end{aligned}$$

Note that for the equilibrium case $\beta = 0$, the current flow is zero, in agreement with the plots of the simulation results (Fig. 2c). By using the adiabatic approximation and the steepest descend method, we have

$$\dot{W} \approx \int_0^{m_0} dm \int_0^1 da \frac{J_m^2}{\Delta_m P} \approx \beta^2\omega_m \frac{\Delta_a/\omega_a}{\Delta_m/\omega_m}(1+\frac{\Delta_m/\omega_m}{\Delta_a/\omega_a}G')^2 \tag{S20}$$

By defining $C_0 = \frac{\Delta_a/\omega_a}{\Delta_m/\omega_m}(1+\frac{\Delta_m/\omega_m}{\Delta_a/\omega_a}G')^2$, we have the following error energy relation

$$\frac{\dot{W}}{C_0\omega_m} \approx \frac{1}{(1+\epsilon_3/e_0)^2}. \tag{S21}$$

By writing $\epsilon_3 = e^x$ and $e_0 = e^{x_0}$, and noting that $\partial^2\dot{W}/\partial x^2 = 0$ at $x = x_0 - \log(2)$, we find that around $\epsilon_3 = e_0/2$ the relation above is logarithmic to second order:

$$\frac{\dot{W}}{C_0\omega_m} \approx \frac{1}{(1+e^{x-x_0})^2} \approx \frac{4}{9} - \frac{8}{27}(x-x_0+\log(2)) + \mathcal{O}(x-x_0)^3 \tag{S22}$$

Finally, by defining $\epsilon_{0,b} = e^{3/2}e_0/2$, $c_{0,b} = 8C_0\omega_a/27\Delta_a$, and $\sigma_a^2 = \Delta_a/\omega_a$ the variance of the variable $a$, we have

$$\dot{W} \approx (c_{0,b}\sigma_a^2) \times \omega_m \times \ln(\frac{\epsilon_{0,b}}{\epsilon_3}), \tag{S23}$$

which has the same form as the ESA relation for the $\beta = 1$ case but with different constants $c_{0,b}$ and $\epsilon_{0,b}$.

# 4 The effect of one-step reaction approximation on the energy dissipation rate

Consider the full Michaelis-Menten reaction $E + S \rightleftarrows ES \rightarrow E + P$ with forward rate $k_f$, backward rate $k_b$, production rate $k_p$. For the convenience of computing the energy dissipation rate, we also introduce a counter-production rate $k_{cp}$ from $E + P$ back to $ES$. The four fluxes can be expressed as:

$$J_f = k_f[E][S],\ J_b = k_b[ES],\ \ J_p = k_p[ES],\ \ J_{cp} = k_{cp}[E][P],$$

where $[E]$, $[S]$, $[P]$, $[ES]$ are concentrations for enzyme, substrate, product, and enzyme-substrate complex respectively. The net flux $J$ is $J = J_f - J_b = J_p - J_{cp}$. The energy dissipation rate $\dot{W}_b$ over the substrate-enzyme binding/unbinding reactions is: $\dot{W}_b = (J_f - J_b)\ln(J_f/J_b) = J\ln(1 + J/J_b)$. The energy dissipation rate over the production/counter-production reactions is: $\dot{W}_p = (J_p - J_{cp})\ln(J_p/J_{cp}) = J\ln(1 + J/J_{cp})$. Here, the thermal energy unit $kT = 1$.

The production step is highly irreversible, so $J_{cp} \ll J$, and $J \approx J_p = k_p[ES]$. For Michaelis-Menten reactions, the substrate is in fast chemical equilibrium with the complex, i.e., $k_b \gg k_p$, so $J/J_b \approx J_p/J_b = k_p/k_b \ll 1$. Finally, the ratio between the two energy dissipation rates is obtained:

$$\frac{\dot{W}_b}{\dot{W}_p} = \frac{\ln(1 + J/J_b)}{\ln(1 + J/J_{cp})} \approx \frac{J}{J_b \ln(J/J_{cp})} \ll \frac{J}{J_b} \approx k_p/k_b \ll 1.$$

This shows that the energy dissipation rate over the substrate-enzyme binding-unbinding process is negligible in comparison with the energy dissipation rate over the production process in any Michaelis-Menten reactions. Therefore, the one-step reaction approximation used in the paper is valid in determining the energy dissipation rates of the methylation/demethylation processes, which are known to be Michaelis-Menten reactions.

# 5 The error-energy dissipation relationship in *E. coli* chemotaxis and its dependence on key system parameters

The relationship between the adaptation error ($\epsilon$) and the energy dissipation ($\Delta W \equiv \dot{W} k_R^{-1}$) is shown in Figure 3c in the main text.

$$\epsilon = \epsilon_0 \times e^{-\alpha \Delta W}, \quad \Delta W \ll \Delta W_c, \tag{S24}$$

$$= \epsilon_c, \qquad \Delta W \gg \Delta W_c. \tag{S25}$$

The system operates along the optimum $\epsilon - \Delta W$ line as more energy dissipation reduces adaptation error. The prefactor $\alpha$ in the exponential $\epsilon - \Delta W$ relation (Eq. S24) depends on the ratio of the two kinetic enzymatic rates $k_R$ and $k_B$ as shown in Fig. S1. In fact, $\alpha$ can be expressed as: $\alpha = (1 + k_R/k_B)/2$, as presented in the main text (Fig. 3d) and proven explicitly in the simple case of a 4-state model in this SI.

Other than $\alpha$, the overall $\epsilon - \Delta W$ relationship is characterized by $\Delta W_c$ and $\epsilon_c$. When energy dissipation $\Delta W$ is bigger than a critical value $\Delta W_c$, the $\epsilon - \Delta W$ curve becomes flat and the adaptation error saturates at a minimum error $\epsilon_c$. We define the critical $\Delta W_c$ to be the energy dissipative rate to achieve an adaptive error within 1% of its saturation value $|1 - \epsilon/\epsilon_c| = 1\%$.

The saturation error $\epsilon_c$ is caused by the adaptation failure at the methylation boundaries ($m = 0, m = m_0$). Specifically, For a receptor with $m = 0$, CheB-P can not demethylate it any further, and so is the case for CheR with receptors with $m = m_0 = 4$. Quantitatively, when $\gamma = 0$, i.e., $\Delta W \to \infty$, the total methylation and demethylation fluxes can be expressed as:

$$J_+ = k_R \sum_{m=0}^{m_0-1} P_0(m) = k_R[(1 - \langle a \rangle) - P_0(m_0)], \tag{S26}$$

$$J_- = K_B \sum_{m=1}^{m_0} P_1(m) = k_B[\langle a \rangle - P_1(0)], \tag{S27}$$

where $P_a(m)$ is the probability of the receptor in state $(a, m)$, and we have used the fact the average activity can be expressed as $\langle a \rangle = \sum_{m=0}^{m_0} P_1(m)$ and correspondingly $1 - \langle a \rangle = \sum_{m=0}^{m_0} P_0(m)$. In steady state, these two fluxes are equal $J_+ = J_-$, which leads to:

$$\langle a \rangle = a_0 + (1 - a_0)P_1(0) - a_0 P_0(m_0), \tag{S28}$$

from which we obtain the saturation error, i.e., the error at $\gamma = 0$:

$$\epsilon_c = |(1/a_0 - 1)P_1(0) - P_0(m_0)|. \tag{S29}$$

Here in this section, we describe in detail how $\Delta W_c$ and $\epsilon_c$ depends on the key system parameters such as the relative reaction time scales in the activity switching direction ($\tau_a$) comparing to the methylation direction ($k_R^{-1}$), and energy gaps at the methylation boundaries ($\Delta E(0)$ and $\Delta E(m_0)$).

## 5.1 The dependence on the activity switching time $\tau_a$

Here, we study how the speed of activity switching (measured by $\tau_a$) affects adaptation by determining the adaptive error as a function of dissipated energy at $\tau_a = 100$, 10, 1, 0.1, $0.01k_R^{-1}$ for ligand concentrations $s = 10^{-2}$, $10^1$ and $10^4 K_I$ (FIG S2a). For each given $s$,

the $\epsilon - \Delta W$ performance curves at different $\tau_a$ values are overlapping until the individual critical saturation point $(\epsilon_c, \Delta W_c)$ is reached.

We then varies $\tau_a$ over a broader range from $10^{-3} \times k_R^{-1}$ to $10^6 \times k_R^{-1}$. Result clearly shows that slower activity switching speed (larger $\tau_a$) lowers adaptive accuracy (larger $\epsilon_c$) and decreases the critical dissipative energy (smaller $\Delta W_c$). This suggests that slower activity switching limit the ability of the chemotaxis system to use energy for adaptation that makes the $\epsilon - \Delta W$ scaling reaches its saturation faster. When activity switching happens too slow ($\tau_a > 10^3 k_R^{-1}$), the system completely loses its ability to adapt (FIG S2b&c). In addition, slower activity switching increases the percentage of amount of energy dissipated in the activity direction. Under certain condition, this percentage can be more than 50% (as shown in FIG S2d). These results implies that activity switching acts as a "valve" in the adaptation circuit: when the "valve" is open (fast switching), two enzymes CheR and CheB can use SAM energy to generate net probability flux to maintain adaptation; however, for large $\tau_a$, the system is jammed as the net transitional flux is limited by the slow activity switching. This jamming effect at large $\tau_a$ increases $P_0(m_0)$ and $P_1(0)$, which compromises the feedback control mechanism and therefore lowers the adaptation accuracy.

## 5.2 The dependence on the boundary energy differences $\Delta E(0)$ and $\Delta E(m_0)$

As shown in the main text, the saturation error $\epsilon_c$ can come from the receptor populations at the two methylation boundary states: $(a = 1, m = 0)$ and $(a = 0, m_0)$, where CheB and CheR can not perform their normal "feedback" actions. Approximately, we have $\epsilon_c = |(a_0^{-1} - 1)P_1(0) - P_0(m_0)|$. Due to fast equilibration in the $a-$ direction, we have $P_0(m_0) \approx P(m_0)(1 + \exp(-\Delta E(s, m_0))^{-1}$, $P_1(0) \approx P(0)(1 + \exp(\Delta E(s, 0))^{-1}$. Therefore increasing the energy difference (gap) at the two boundaries ($m = 0$ and $m = m_0$) can reduce $P_1(0)$ and $P_0(m_0)$, and consequently $\epsilon_c$. Here, we verify this result by direct simulation of our discrete model.

To study the dependence of $\epsilon_c$ on the intrinsic energy difference of the active and inactive receptor with $s = 0$, we denote $\Delta E(m)$ as the part of $\Delta E(s, m)$ that only depends on $m$, $\Delta E(m)$ is also called the methylation energy. We study the depdence of adaptation accuracy on the boundary methylation energies $\Delta E(0)$ and $\Delta E(m_0)$.

Since the adaptation errors from the two boundaries have opposite signs, for intermediate ligand concentrations, populations at the two boundaries can be comparable, and these two errors could spuriously cancel each other. To get the "uncontaminated" dependence on an individual boundary energy gap, e.g., $m = 0$, we set the other energy gap $\Delta E(m_0)$ to be essentially infinity to have $P_0(m_0) = 0$, and the ligand concentration $(s)$ is chosen so that $P(0)$ is finite: for the $m = 0$ boundary, we choose low ligand concentrations $(s < K_I)$, and for the $m = m_0$ boundary, we choose high ligand concentrations

($s > K_A$). We determine the $(\epsilon_c, \Delta W_c)$ values for each choice of the energy gap. The results are shown in Fig. S3, which shows clearly that increasing $|\Delta E(0)|$ and $|\Delta E(m_0)|$ decreases the saturation error $\epsilon_c$ exponentially (Fig. S3a&c), and the saturation energy $\Delta W_c$ increases linearly $|\Delta E(0)|$ and $|\Delta E(m_0)|$ (Fig. S3a&c).

# References

[1] Hong Qian. Phosphorylation energy hypothesis: Open chemical systems and their biological functions. *Annu. Rev. Phys. Chem.*, 58:113–142, Oct 2007.

[2] J. L. Lebowitz and H. Spohn. A Gallavotti-Cohen-type symmetry in the large deviation funcional for stochastic dynmaics. *Journal of Statistical Physics*, 95(1-2):1572–9613, 1999.

[3] T. Tome. Entropy production in nonequilibrium systems described by a Fokker-Planck equation. *Brazilian Journal of Physics*, 36(4A):1285–1289, 2006.

## Movie Legend

Movie S1: Adaptation kinetics in phase space. An animation of the state distribution $P(a, m, t)$ and the corresponding flux field in response to a step increase of $s$ (from $s = 10$ to $s = 10^3$ at time=1(a.u.)) is produced with 36 frames in the animated gif format. $G = [1 + (s/K_d(m))]^{-1}$ with $K_d = K_0 e^{2m}$ and $K_0 = 1$, see Methods in main text for other parameters.

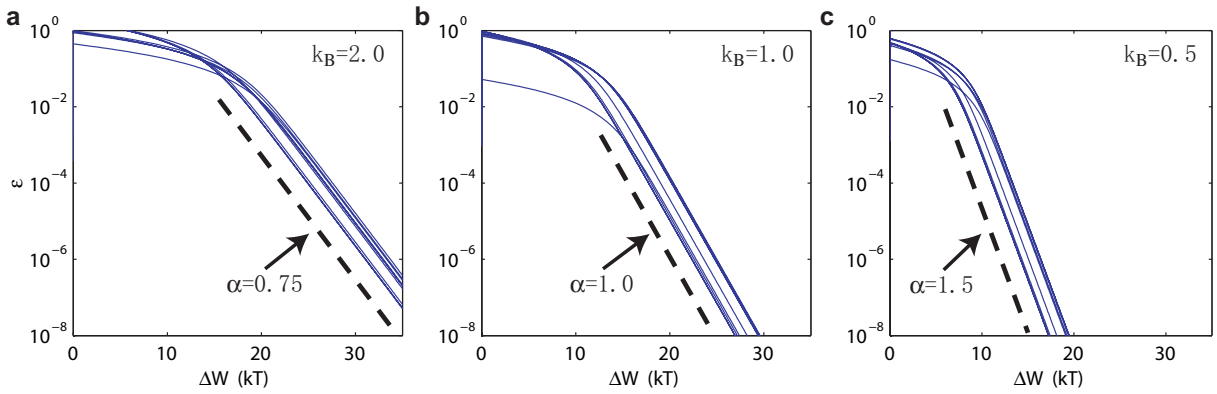


Figure S1: The dependence of $\alpha$ on the $k_B/k_R$ ratio. $k_R = 1$ is set to be unit to set the time scale. The $\epsilon - \Delta W$ curves are computed for three different choices of $k_B$: **a.** $k_B = 2.0$; **b.** $k_B = 1.0$; **c.** $k_B = 0.5$. $\alpha$ can be determined by the slope of the semi-log plot, its values are 0.75, 1.0, 1.5 for the three cases shown here, and they agree with the expression $\alpha = (1 + k_R/k_B)/2$.

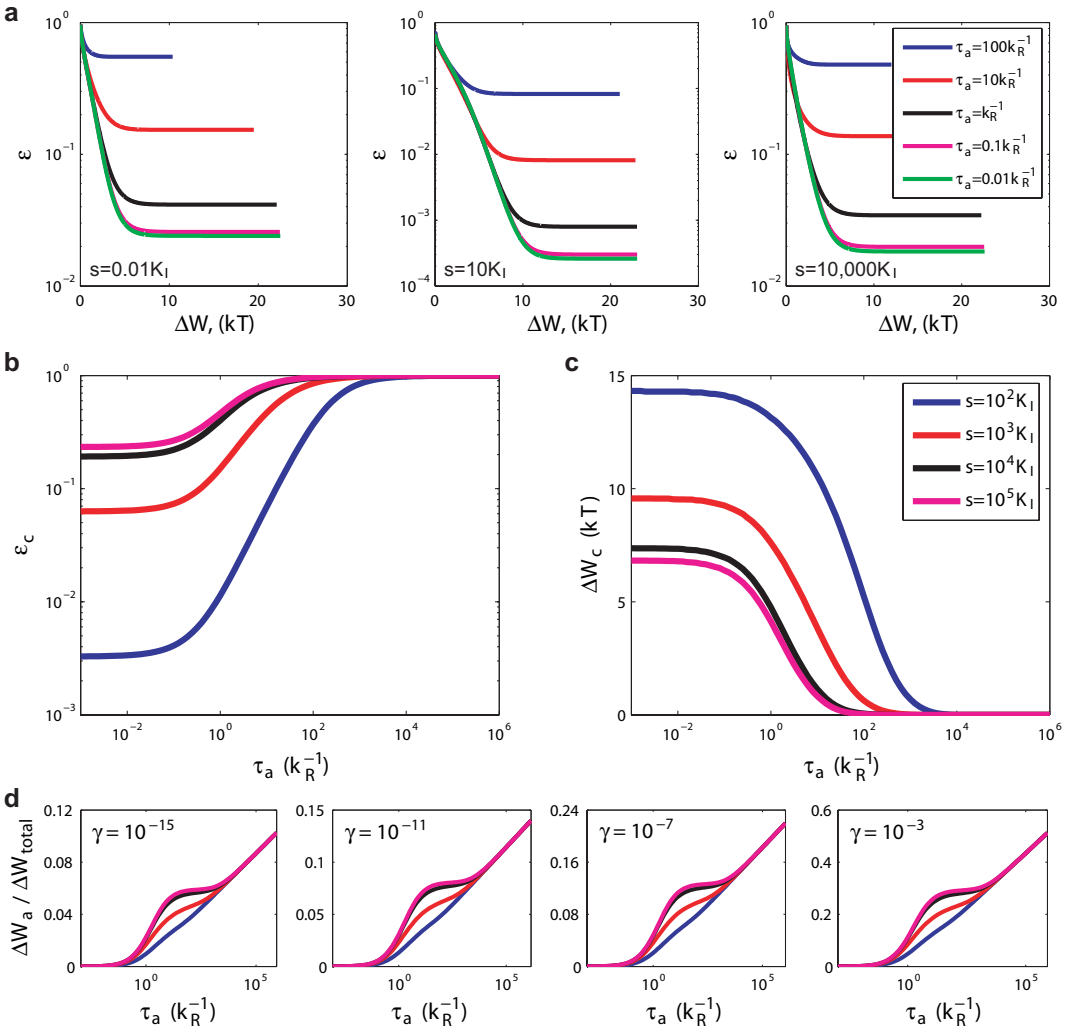


Figure S2: The effects of receptor activation time $\tau_a$. **a.** $\epsilon - \Delta W$ curves at different signal strength (ligand concentration) $s = 0.01K_I$, $10K_I$ and $10000K_I$ when the receptor activation time varies from $\tau_a = 0.01K_R^{-1}$ to $\tau_a = 100K_R^{-1}$. At different $s$, a smaller $\tau_a$ improves adaptation accuracy as the $\epsilon - \Delta W$ curve saturates at a lower critical error $\epsilon_c$ along the same performance line. The dependence of the saturation error $\epsilon_c$ and its corresponding energy dissipation $\Delta W_c$ on $\tau_a$ are shown in **b&c**. $\epsilon_c$ increases with $\tau_a$ while $\Delta W_c$ decreases with $\tau_a$. When $\tau_a$ goes below $0.01k_R^{-1}$, the error does not improve as the system is already in the fast equilibration regime in the $a-$direction. When $\tau_a > 1000k_R^{-1}$, the system totally loses its ability to adapt due to the slow activation process. **d.** The percentage of energy dissipated in $a-$direction ($\Delta W_a$) over the total amount of dissipated energy. This percentage increases when $\tau_a$ increases.

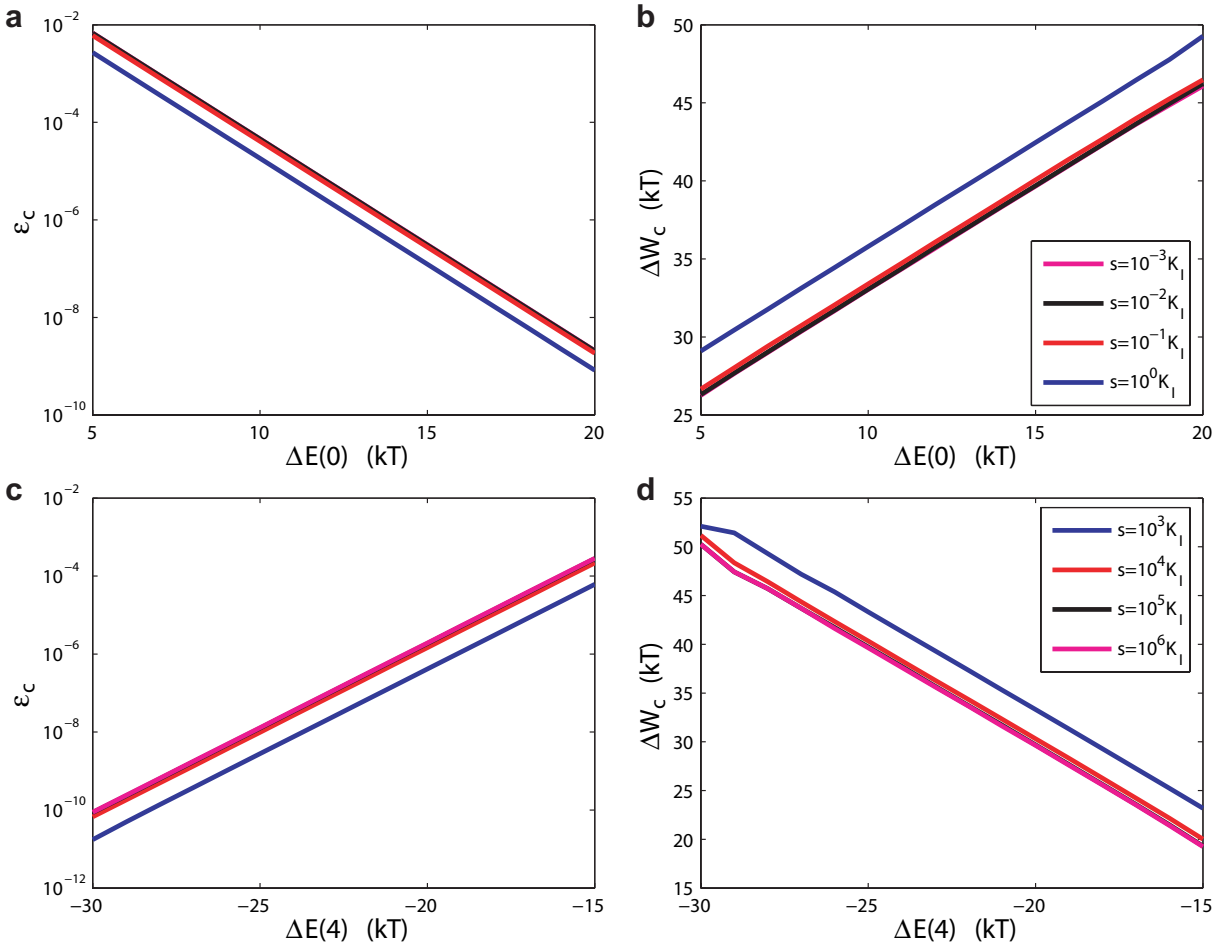


Figure S3: Energy gaps $\Delta E(0)$ and $-\Delta E(4)$ controls the saturation (minimum) adaptation error $\epsilon_c$ and the critical dissipative energy $\Delta W_c$. **a.** $\epsilon_c$ and **b.** $\Delta W_c$ versus $\Delta E(0)$ (keeping $\Delta E(4) = -\infty$). **c.** $\epsilon_c$ and **d.** $\Delta W_c$ versus $\Delta E(4)$ (keeping $\Delta E(0) = \infty$). Increasing energy gaps $|\Delta E(0)|$ and $|\Delta E(4)|$ reduces $\epsilon_c$ exponentially. The system needs to dissipate more energy $\Delta W_c$, linearly proportional to $|\Delta E(0)|$ and $|\Delta E(4)|$, to reach the saturation error $\epsilon_c$. Differently colored lines in each panel are for different values of signal strength $s$.